

**QUALITATIVE AND QUANTITATIVE
ACCURACY EVALUATION OF ^{18}F -FDG PET/CT
WITH TOF AND NON-TOF SYSTEM ON BETA
VALUE IN BPL RECONSTRUCTION**

NG SUK HUI

SCHOOL OF HEALTH SCIENCES

UNIVERSITI SAINS MALAYSIA

2024

**QUALITATIVE AND QUANTITATIVE
ACCURACY EVALUATION OF ^{18}F -FDG PET/CT
WITH TOF AND NON-TOF SYSTEM ON BETA
VALUE IN BPL RECONSTRUCTION**

by

NG SUK HUI

**Dissertation submitted in partial fulfilment of the requirements for the degree of
Bachelor of Health Science (Honours) (Medical Radiation)**

July 2024

CERTIFICATE

This is to certify that the dissertation entitled “QUALITATIVE AND QUANTITATIVE ACCURACY EVALUATION OF ^{18}F -FDG PET/CT WITH TOF AND NON-TOF SYSTEM ON BETA VALUE IN BPL RECONSTRUCTION” is the bona fide record of research work done by Ms “NG SUK HUI” during the period from October 2023 to July 2024 under our supervision. We have read this dissertation and that in our opinion it conforms to acceptable standards of scholarly presentation and is fully adequate, in scope and quality, as a dissertation to be submitted in partial fulfilment for the degree of Bachelor of Health Science (Honours) (Medical Radiation).

Main supervisor,

.....
Dr. Marianie Binti Musarudin

University Lecturer

School of Health Sciences

Universiti Sains Malaysia

Health Campus

16150 Kubang Kerian

Kelantan, Malaysia

Date:

Co-supervisor,

.....
Dr. Mohammad Khairul Azhar
Abdul Razab

Chairperson

Medical Radiation Program

School of Health Sciences

Universiti Sains Malaysia

Health Campus

16150 Kubang Kerian

Kelantan, Malaysia

Date:

Co-supervisor,

.....
Dr. Mohamad Aminudin Bin Said
Medical Science Officer (Physics)
Nuclear Medicine Department
Institut Kanser Negara
4, Jalan P7, Presint 7,
62250 Putrajaya,
Wilayah Persekutuan Putrajaya
Date:

Field supervisor,

.....
Pn. Ummi Habibah binti Ibarhim
Medical Science Officer (Physics)
Nuclear Medicine Department
Institut Kanser Negara
4, Jalan P7, Presint 7,
62250 Putrajaya,
Wilayah Persekutuan Putrajaya
Date:

DECLARATION

I hereby declare that this dissertation is the result of my own investigations, except where otherwise stated and duly acknowledged. I also declare that it has not been previously or concurrently submitted as a whole for any other degrees at Universiti Sains Malaysia or other institutions. I grant Universiti Sains Malaysia the right to use the dissertation for teaching, research and promotional purposes.

.....

NG SUK HUI

Date:

ACKNOWLEDGEMENT

This work owes its success to the invaluable contributions of several individuals, whom I am deeply grateful to acknowledge.

Firstly, I extend my heartfelt gratitude to Dr. Marianie Binti Musarudin, my main supervisor at the School of Health Science, Health Campus of Universiti Sains Malaysia (USM), for her in-depth knowledge of all things colloidal. Throughout my final year project journey, her patience, encouragement, and invaluable advice have been truly appreciated. Besides, Dr. Mohammad Khairul Azhar Abdul Razab, also a lecturer from USM, deserves special recognition for generously sharing his expertise and providing valuable feedback that significantly enhanced the quality of my thesis.

I would like to express my deep appreciation to Dr. Mohamad Aminudin Bin Said, head physicist of the Nuclear Medicine Department at Institut Kanser Negara (IKN), for inviting me and providing necessary facilities to undertake this study under his guidance. His valuable advice and insightful discussions were instrumental in the success of this endeavour. Furthermore, I am also indebted to Puan Umami Habibah binti Ibarhim, a medical physicist at Nuclear Medicine Department at IKN, for her generous sharing of knowledge and invaluable assistance in data collection.

Special thanks are extended to Dr. Faridah Naim, a lecturer at the School of Health Science, USM, for her continuous support, expertise in statistical analysis, and patience in guiding me through my study. Besides, I am deeply grateful to my family members and friends for their unwavering encouragement and support throughout this journey. Lastly, I also acknowledge the contributions of all those who directly or indirectly assisted in this venture.

TABLE OF CONTENTS

CERTIFICATE	ii
DECLARATION	iv
ACKNOWLEDGEMENT	v
TABLE OF CONTENTS	vi
LIST OF TABLES	x
LIST OF FIGURES	xii
LIST OF SYMBOLS	xv
LIST OF ABBREVIATIONS	xvii
LIST OF APPENDICES	xix
ABSTRAK	xx
ABSTRACT	xxii
CHAPTER 1	1
INTRODUCTION	1
1.1. Background of the Study	1
1.2. Problem Statement.....	3
1.3. Study Objective.....	4
1.3.1. General Objective	4
1.3.2. Specific Objectives	4
1.4. Study Hypothesis	4
1.4.1. Null Hypothesis	4
1.4.2. Alternative Hypothesis	5
1.5. Significance of the Study	5
CHAPTER 2	7
LITERATURE REVIEW	7
2.1. PET Imaging	7
2.1.1. PET Radiotracers	7
2.1.2. PET/CT Integration.....	9

2.2.	Qualitative accuracy of PET/CT.....	12
2.2.1.	PET/CT Image Quality	12
2.3.	Quantification accuracy of PET/CT	13
2.3.1.	Quantitative metrics of PET/CT	14
2.4.	Factors affecting PET Image	17
2.4.1.	Radiotracer properties and dose administration.....	17
2.4.2.	Reconstruction algorithm and parameters	18
2.4.3.	Partial Volume Effect (PVE)	24
CHAPTER 3	27
METHODOLOGY	27
3.1.	Study Flowchart.....	27
3.2.	Materials	28
3.2.1.	PET/CT GE Healthcare Discovery MI DR.....	28
3.2.2.	PET image quality phantom: NEMA 2012/ IEC 2018.....	30
3.2.3.	Dose Calibrator: Atomlab™ 500.....	31
3.2.4.	¹⁸ F-FDG	32
3.2.5.	Micro-lead and 50-cc syringe	33
3.2.6.	MIM Encore Software	33
3.3.	Methods	34
3.3.1.	Preparation of the Phantom.....	34
3.3.2.	PET/CT Image Acquisition	38
3.3.3.	PET/CT Reconstruction.....	41
3.3.4.	Quantitative Image Evaluation	42
3.3.5.	Qualitative Image Evaluation	44
3.4.	Data Analysis.....	45
3.4.1.	Statistical Analysis for Quantitative Metrics	45
3.4.2.	Statistical Analysis for Qualitative Metrics	46
3.5.	Ethical Clearance	46
CHAPTER 4	47

RESULTS	47
4.1. Preparation of phantom.....	47
4.2. Quantitative Image Evaluation	47
4.2.1. Recovery Coefficient (RC)	48
4.2.2. Coefficient of Variance (COV).....	50
4.2.3. Contrast-to-Noise Ratio (CNR)	51
4.3. Qualitative Image Evaluation	55
4.4. Data Analysis.....	56
4.4.1. Statistical Analysis for Quantitative Metrics	56
4.4.2. Statistical Analysis for Qualitative Metrics	60
CHAPTER 5	62
DISCUSSION	62
5.1. Discussion.....	62
5.1.1. Recovery Coefficient (RC)	62
5.1.2. Coefficient of Variance (COV).....	64
5.1.3. Contrast-to-Noise Ratio (CNR)	66
5.1.4. Qualitative Analysis.....	67
5.1.5. Reconstruction Algorithm Analysis.....	69
5.2. Limitation of Study	71
CHAPTER 6	73
CONCLUSION	73
6.1. Overall findings of this study.....	73
6.2. Future recommendation	74
REFERENCES	76
APPENDICES	84
APPENDIX A	84
APPENDIX B	85
APPENDIX C	89
APPENDIX D	94

APPENDIX E..... 97
APPENDIX F..... 98
APPENDIX G..... 100

LIST OF TABLES

Table 3.1: PET system specifications for GE Discovery MI DR system	29
Table 3.2: Physical properties of ^{18}F radioisotopes (Jacobson <i>et al.</i> , 2015).....	32
Table 3.3: Total amount of ^{18}F activity required for hot spheres and background.....	35
Table 3.4: Assumption of activity required, decay constant, time interval between phantom preparation and image acquisition of ^{18}F for both sphere and background	36
Table 3.5: Calculated initial activity of ^{18}F required for spheres and background.....	36
Table 3.6: New initial activity of ^{18}F required.....	37
Table 3.7: Parameters of PET/CT image acquisition	40
Table 3.8: Overview of image reconstruction (OSEM and BPL algorithms) parameters	41
Table 3.9: 4-point rating scale for sphere detectability and noise level (Teoh <i>et al.</i> , 2018; Wang <i>et al.</i> , 2022).....	44
Table 4.1: Activity concentration of spheres and background of ^{18}F	47
Table 4.2: Comparison of mean RC_{max} between TOF and non-TOF in BPL and OSEM reconstruction algorithm	57
Table 4.3: Comparison of median RC_{max} between TOF and non-TOF in BPL reconstruction algorithm	58
Table 4.4: Comparison of mean CNR_{mean} between TOF and non-TOF in BPL reconstruction algorithm	58
Table 4.5: Comparison of median CNR_{mean} between TOF and non-TOF in OSEM reconstruction algorithm	59
Table 4.6: Comparison of mean CNR_{max} between TOF and non-TOF in BPL and OSEM reconstruction algorithm	59

Table 4.7: Comparison of median CNR_{max} between TOF and non-TOF in BPL reconstruction algorithm	59
Table 4.8: Cohen’s Kappa coefficient results for the sphere detectability scores	60
Table 4.9: Cohen’s Kappa coefficient results for the noise levels scores.....	61
Table C.1: RC_{max} values for both TOF and non-TOF PET/CT in OSEM and BPL reconstruction with beta values ranging from 100 to 2000	89
Table C.2: COV values for both TOF and non-TOF PET/CT in OSEM and BPL reconstruction with beta values ranging from 100 to 2000	90
Table C.3: CNR_{mean} values for both TOF and non-TOF PET/CT in OSEM and BPL reconstruction with beta values ranging from 100 to 2000	91
Table C.4: CNR_{max} values for both TOF and non-TOF PET/CT in OSEM and BPL reconstruction with beta values ranging from 100 to 2000	92
Table D.1: Sphere detectability scores for both TOF and non-TOF PET/CT images reconstructed with OSEM and BPL (beta values ranging from 100 to 2000) reconstructions	94
Table D.2: Noise level scores for both TOF and non-TOF PET/CT images reconstructed with OSEM and BPL (beta values ranging from 100 to 2000) reconstructions	95
Table E.1: The results of Shapiro-Wilk normality test for RC_{max} , CNR_{mean} and CNR_{max}	97

LIST OF FIGURES

Figure 2.1: Process flow maps for conventional OSEM iterative reconstruction and Q.Clear (Ross, n.d.).	21
Figure 2.2: Schematic illustration of conventional PET and TOF PET (Brusaferrri, 2020).	24
Figure 3.1: Study flowchart.	27
Figure 3.2: GE Healthcare PET/CT Discovery MI DR.	29
Figure 3.3: NEMA image quality phantom with a lung insert and six fillable spheres of known internal diameters.	30
Figure 3.4: Atomlab™ 500 dose calibrator.	31
Figure 3.5: ¹⁸ F-FDG in a vial (Left) and syringe (Right).	32
Figure 3.6: ¹⁸ F-FDG stored in a PET vial pig (lead shield).	32
Figure 3.7: A 50-cc syringe filled with a mixture of blue-dyed tap water and ¹⁸ F-FDG, attached with a micro-lead.	33
Figure 3.8: Preparation of a mixture of ¹⁸ F-FDG with blue-dyed tap water in a glass bottle.	38
Figure 3.9: Preparation of the phantom for the background section, showing the filling of tap water (Left) and the injection of measured ¹⁸ F-FDG prepared in a syringe (Right).	38
Figure 3.10: Actual phantom positioning during PET/CT image acquisition.	39
Figure 3.11: Laser alignment for phantom positioning.	39
Figure 3.12: Illustration of phantom positioning during PET/CT image acquisition.	40
Figure 3.13: Selection of FDG PET/CT whole-body “Motion Free” “Q.Static” (FDG PETCT WB MF QS) protocol.	40
Figure 3.14: PET reconstruction type window.	41

Figure 3.15: ROI delineation (6 spheres and 11 backgrounds) in MIM Encore software for BPL 450 reconstructed image.	42
Figure 4.1: A combined clustered column chart with line comparing the RC_{max} of BPL across various beta values and OSEM algorithms, with TOF acquisition.....	49
Figure 4.2: A combined clustered column chart with line comparing the RC_{max} of BPL across various beta values and OSEM algorithms, with non-TOF acquisition.	49
Figure 4.3: The RC_{max} computed for different spheres diameter groups (13 mm and 13-37 mm) in BPL across various beta values, comparing TOF and non-TOF acquisitions.	50
Figure 4.4: A combined clustered column chart with line comparing the COV of TOF and non-TOF acquisitions in OSEM and BPL algorithm across various beta values.	51
Figure 4.5: A combined clustered column chart with line comparing the CNR_{mean} of BPL across various beta values and OSEM algorithms, with TOF acquisition.....	53
Figure 4.6: A combined clustered column chart with line comparing the CNR_{max} of BPL across various beta values and OSEM algorithms, with TOF acquisition.....	53
Figure 4.7: A combined clustered column chart with line comparing the CNR_{mean} of BPL across various beta values and OSEM algorithms, with non-TOF acquisition.	54
Figure 4.8: A combined clustered column chart with line comparing the CNR_{max} of BPL across various beta values and OSEM algorithms, with non-TOF acquisition.	54
Figure 4.9: Scatter chart comparing the CNR values between TOF and non-TOF BPL acquisitions in 10 mm and 13-37 mm sphere groups.	55
Figure 4.10: A combined clustered column chart with line comparing the visual score between TOF and non-TOF acquisitions for sphere detectability and noise level.....	56
Figure A.1: Setup of NEMA uniform phantom for sensitivity test.	84
Figure A.2: Sensitivity of PET/CT system as conversion factor.....	84
Figure B.1: PET performance specifications of PET/CT scanner.	85
Figure B.2: CT performance specifications of PET/CT scanner.	86

Figure B.3: Advanced quantitative reconstructions of PET/CT system.	87
Figure B.4: Intelligent motion management of PET/CT system.	88
Figure F.1: PET images reconstructed with different beta value in BPL reconstruction with TOF acquisition.	98
Figure F.2: PET images reconstructed with different beta value in BPL reconstruction with non-TOF acquisition.	99
Figure F.3: PET images reconstructed with OSEM reconstruction with TOF (Left) and non-TOF acquisition (Right).	99
Figure G.1: Ethical review statement from MREC.	100

LIST OF SYMBOLS

^{11}C	Carbon-11
^{137}C	Caesium-137
^{18}F	Fluorine-18
^{68}Ga	Gallium-68
^{177}Lu	Lutetium-177
^{18}O	Oxygen-18
A	Activity of radionuclide
A_0	Initial Activity of radionuclide
AC_{\max}	Maximum Activity Concentration in Bq mL^{-1}
AC_{mean}	Mean Activity Concentration in Bq mL^{-1}
B_{known}	True Activity Concentrations of Background in Bq mL^{-1}
B_{measured}	Global Mean Activity Concentration measured on eleven ROIs of Background in Bq mL^{-1}
CNR_{\max}	Contrast-to-Noise Ratio derived from Maximum Activity Concentration
CNR_{mean}	Contrast-to-Noise Ratio derived from Mean Activity Concentration
λ	Decay Constant
$\sigma_{\text{ROI,bg}}$	Standard Deviation of Activity Concentration in each background ROI
S_{known}	True Activity Concentrations of Hot Sphere in Bq mL^{-1}
S_{measured}	Maximum Activity Concentration measured for the ROI on Hot Sphere in Bq mL^{-1}
IQR	Interquartile Range
κ	Cohen's Kappa Coefficient

μ	Linear Attenuation Coefficients
RC_{\max}	Recovery Coefficient derived from Maximum Activity Concentration
SD	Standard Deviation
$S_{\text{mean}/\max}$	Mean/ Maximum Activity Concentration for the ROI on the Hot Sphere
SUV_{\max}	Maximum Standardised Uptake Value
SUV_{mean}	Mean Standardised Uptake Value
SUV_{peak}	Peak Standardised Uptake Value
t	Decay time
$T_{1/2}$	Half-life

LIST OF ABBREVIATIONS

3D	3-Dimensional
ATP	Adenosine Triphosphate
BMI	Body Mass Index
BPL	Bayesian Penalised Likelihood
BSREM	Block Sequential Regularised Expectation Maximisation
CNR	Contrast-to-Noise Ratio
COV	Coefficient of Variance
CT	Computed Tomography
DOPA	L-dihydroxyphenylalanine
DOTA-TATE	DOTA-DPhe ¹ -Tyr ³ -Octreotate
EANM	European Association of Nuclear Medicine
FDG	Fluoro-2-deoxy-D-glucose
GE	General Electric
HCl	Hydrochloric Acid
HU	Hounsfield Unit
IEC	International Electrotechnical Commission
IKN	Institut Kanser Negara
IQR	Interquartile Range
LYSO	Lutetium Yttrium Orthosilicate
MET	Methionine
MF	Motion Free
MRI	Magnetic Resonance Imaging
NEMA	National Electrical Manufacturers Association
OSEM	Ordered Subset Expectation Maximisation

PET	Positron Emission Tomography
PSF	Point Spread Function
PSMA	Prostate-Specific Membrane Antigen
PVE	Partial Volume Effect
QS	Q.Static
RC	Recovery Coefficient
RDP	Relative Difference Penalty
ROI	Region of Interest
SiFAlin-TATE	Silicon Fluoride Acceptor tagged Tyr ³ -octreotate
SNR	Signal-to-Noise Ratio
SPSS	Statistical Package for Social Sciences
SUV	Standardised Uptake Value
TBR	Tumour-to-Background
TNM	Tumour, Nodes, and Metastases
APPENDIX G	Time-of-Flight
VPFx	VUE Point HD
VPHD	VUE Point FX
WB	Whole-Body

LIST OF APPENDICES

APPENDIX A	Sensitivity of PET/CT system
APPENDIX B	Technical specifications of GE Healthcare Discovery MI DR PET/CT
APPENDIX C	Quantitative metrics (RC_{\max} , COV, CNR_{mean} , CNR_{\max}) in both TOF and non-TOF PET/CT
APPENDIX D	Results of subjective image quality ratings in both TOF and non-TOF PET/CT reconstructed images
APPENDIX E	Normality test results
APPENDIX F	PET images reconstructed with different beta value in BPL reconstruction with TOF and non-TOF acquisition.
APPENDIX G	Ethical review documentation: Evidence of no further MREC review requirement

PENILAIAN KETEPATAN KUALITATIF DAN KUANTITATIF ¹⁸F-FDG PET/CT DENGAN SISTEM TOF DAN NON-TOF PADA NILAI BETA DALAM REKONSTRUKSI BPL

ABSTRAK

Resolusi dan ketepatan kuantitatif tomografi pancaran positron (PET) sangat bergantung kepada algoritma pembangunan imej. Algoritma *Ordered Subset Expectation Maximisation* (OSEM) tidak dapat mencapai konvergen sepenuhnya (*full convergence*) kerana hingar imej bertambah dengan setiap iterasi. Sebaliknya, algoritma *Penalised Likelihood Estimation* pula membolehkan konvergen yang berkesan, memperbaiki kualiti imej dengan meningkatkan kontras dan mengurangkan hingar. *Q.Clear*, algoritma *Bayesian Penalised Likelihood* (BPL), telah menunjukkan kemajuan yang ketara dalam kualiti imej klinikal dan kuantifikasi, terutamanya dalam mengesan keabnormalan halus. Kajian ini membandingkan prestasi BPL dengan OSEM dalam kedua-dua *Time-of-Flight* (TOF) dan *non*-TOF tomografi pancaran positron dengan tomografi komputer (PET/CT). Dengan memvariasikan faktor penalti hingar (nilai beta) yang mengimbangi pengurangan hingar dan resolusi, kajian ini bertujuan untuk menentukan nilai beta optimum bagi algoritma BPL, terutamanya dalam meningkatkan ketepatan diagnostik dan kualiti imej untuk mengesan lesi kecil. **Metodologi:** Fantom kualiti imej *National Electrical Manufacturers Association* (NEMA) yang diisi dengan *Fluorine-18 fluoro-2-deoxy-D-glucose* (¹⁸F-FDG) pada nisbah tumor kepada latar belakang (*tumour-to-background ratio*, TBR) 5:1 telah diimbas menggunakan PET/CT berasaskan lutetium. Imej PET/CT direkonstruksi menggunakan algoritma OSEM (16 subset, 3 iterasi) dan *Q.Clear* (dengan

nilai beta dari 100 hingga 2000). Kedua-dua algoritma termasuk pemodelan *Point Spread Function* (PSF), dengan dan tanpa TOF informasi untuk perbandingan. Imej fantom ini dinilai secara kuantitatif dan kualitatif. Pekali pemulihan (*Recovery Coefficient*, RC), pekali variasi (*Coefficient of Variance*, COV), dan nisbah kontras-ke-hingar (*Contrast-to-Noise Ratio*, CNR) diperoleh untuk menilai kualiti imej dan kebolehsesanan dalam pengesanan lesi. Penilaian kualiti imej secara kualitatif dilakukan oleh tiga ahli fizik berpengalaman. **Keputusan:** Peningkatan nilai beta membawa kepada pengurangan RC_{max} dan COV, dengan TOF menunjukkan nilai RC_{max} dan COV yang lebih tinggi berbanding *non*-TOF. BPL mencapai pemulihan kuantitatif yang lebih tepat dan hingar yang lebih rendah (kecuali untuk BPL 100) berbanding OSEM. Kedua-duanya CNR_{mean} dan CNR_{max} secara umumnya meningkat dengan diameter sfera. Dalam pengambilan TOF PET/CT, CNR_{mean} dan CNR_{max} mencapai puncaknya sekitar BPL 700 sebelum menurun, sementara dalam pengambilan *non*-TOF PET/CT, kedua-duanya memuncak sekitar BPL 1000 dan BPL 2000 masing-masing. Walaupun OSEM secara umum mengekalkan nilai CNR yang setanding dengan algoritma BPL, BPL menunjukkan penambahbaikan, terutamanya dalam mengurangkan hingar dan meningkatkan kontras. Dalam penilaian subjektif, OSEM dan BPL 450 dinilai lebih tinggi dalam kebolehsesanan sfera dalam TOF PET/CT, manakala BPL 2000 dikenali sebagai yang mempunyai skor hingar tertinggi dalam kedua-dua TOF dan *non*-TOF PET/CT. **Kesimpulan:** Kajian ini menunjukkan bahawa nilai beta 450 untuk TOF- dan 300 untuk *non*-TOF PET/CT adalah optimum. Keputusan ini sejajar dengan penggunaan standard algoritma rekonstruksi dalam penggunaan klinikal di Institut Kanser Negara (IKN), di mana BPL 450 dengan TOF PET/CT digunakan.

**QUALITATIVE AND QUANTITATIVE ACCURACY
EVALUATION OF ¹⁸F-FDG PET/CT WITH TOF AND NON-TOF
SYSTEM ON BETA VALUE IN BPL RECONSTRUCTION**

ABSTRACT

The resolution and quantitative accuracy of Positron Emission Tomography (PET) greatly depend on the reconstruction algorithm. Ordered Subset Expectation Maximisation (OSEM) is unable to achieve full convergence as image noise grows with each iteration, potentially compromising quantitative accuracy. Penalised likelihood estimation algorithms, on the other hand, allow for an effective convergence that improves image quality by enhancing contrast and reducing noise. Q.Clear, a Bayesian Penalised Likelihood (BPL) algorithm, has demonstrated notable advancements in clinical image quality and quantification, particularly in detecting subtle abnormalities. This study compares the performance of BPL with OSEM in both Time-of-Flight (TOF) and non-TOF Positron Emission Tomography/ Computed Tomography (PET/CT) acquisitions. By varying the noise penalisation factor (beta value), which balances noise reduction and resolution, the study aims to determine optimal beta value for BPL, particularly in enhancing diagnostic accuracy and image quality for small lesions. **Methods:** A National Electrical Manufacturers Association (NEMA) image quality phantom filled with Fluorine-18 fluoro-2-deoxy-D-glucose (¹⁸F-FDG) at a 5:1 tumour-to-background ratio (TBR) was scanned on a lutetium-based PET/CT scanner. The images were reconstructed using the OSEM (16 subsets, 3 iterations) and Q.Clear algorithms, both of which include Point Spread Function (PSF) modelling. Q.Clear was

investigated for beta values ranging from 100 to 2000. Both BPL and OSEM reconstructions were acquired with and without TOF information for comparison. These phantom images were evaluated quantitatively and qualitatively. The Recovery Coefficient (RC), Coefficient of Variance (COV), and Contrast-to-Noise Ratio (CNR) were measured to evaluate image quality and lesion detectability. Subjective image quality was performed by three experienced physicists. **Results:** Increasing beta values led to reduced RC_{\max} and COV, with TOF acquisitions consistently exhibiting higher RC_{\max} and COV values compared to non-TOF acquisitions. BPL achieved more accurate quantitative recovery and lower noise (except BPL 100) compared to OSEM reconstruction. Both CNR_{mean} and CNR_{\max} generally increased with sphere diameter. In TOF acquisitions, CNR_{mean} and CNR_{\max} peaked around BPL 700, declining thereafter, while in non-TOF acquisitions, both plateaued around BPL 1000 after an initial drop at BPL 100 and BPL 200. While OSEM generally maintained comparable CNR values across various beta values, BPL reconstruction exhibited improvements, particularly in reducing noise and enhancing contrast. In subjective evaluation, OSEM and BPL 450 were rated higher for sphere detectability in TOF acquisition, whereas BPL 2000 was identified as having the highest noise score in both TOF and non-TOF acquisitions. **Conclusion:** Our study findings suggested that a beta value of 450 was optimal for TOF acquisition, while a beta value of 300 was recommended for non-TOF acquisition. These results were consistent with the standard practice at IKN, where a BPL 450 with TOF acquisition is used.

CHAPTER 1

INTRODUCTION

1.1. Background of the Study

Fluorine-18 Fluoro-2-deoxy-D-glucose (^{18}F -FDG) Positron Emission Tomography/ Computed Tomography (PET/CT) is widely used in oncology for diagnosing tumours, monitoring therapy response, and detecting disease recurrence. This non-invasive imaging technique provides valuable insights into physiological and pathological processes in vivo as Fluoro-2-deoxy-D-glucose (FDG) accumulates in areas with high glucose demand (Lindström *et al.*, 2018). Compared to other imaging techniques, Positron Emission Tomography (PET) holds a distinct advantage for its high sensitivity and accuracy. This stems from its unique method of detecting radiation, which involves positron-generated paired 511 keV annihilation photons. With proper calibration and corrections for attenuation, scatter, and random coincidences, PET images can provide quantitative data on local tracer activity, expressed in absolute units as kiloBecquerel per millilitre (kBq mL^{-1}) (Herholz, 2014). Both assessing staging and monitoring treatment outcomes necessitates precise quantification of PET images (Boellaard *et al.*, 2015). However, PET/CT image quality faces challenges primarily due to their limited spatial resolution and Signal-to-Noise Ratio (SNR), which leads to a less robust and reproducible Standardised Uptake Value (SUV).

Several factors have been recognised as impacting the accuracy of quantification and image interpretation in PET/CT. Advances in reconstruction methods contribute significantly to improving image quality. The integration of Time-of-Flight (TOF) information into iterative reconstruction algorithms, results in PET/CT images with higher SNR, which improves the detection of small lesions. The algorithm most often

applied to optimise the Contrast-to-Noise Ratio (CNR) is Ordered Subset Expectation Maximisation (OSEM) reconstruction. However, full convergence is unattainable for OSEM due to the progressive increase in image noise with each iteration. Therefore, a necessary trade-off between iteration and noise leads to partial convergence.

A Bayesian Penalised Likelihood (BPL) algorithm known as Q.Clear has been introduced to tackle the issue of convergence and enhance PET quantification accuracy. This algorithm offers the advantage of activity-dependent noise control and achieves global convergence for all image voxels by using Relative Difference Penalty (RDP) and Block Sequential Regularised Expectation Maximisation (BSREM) approaches respectively. Image noise can be regulated by the penalisation factor, denoted as the beta value. A higher beta value increases the impact of regularisation, effectively suppressing noise (Howard *et al.*, 2017). The widely used beta value of 400 is common in general oncological cases with Lutetium Yttrium Orthosilicate (LYSO) scanners and ^{18}F -FDG (Parvizi *et al.*, 2015; Teoh *et al.*, 2015, 2016). However, it may not consider optimised count statistics or ratios for individual cases. Since the noise penalisation factor controls the trade-off between noise level and resolution, optimal beta values enhance the diagnostic accuracy and image quality, especially for small lesions, which hold significance factor to be considered in the field of nuclear medicine.

This study focuses on selecting the optimal beta values in TOF and non-TOF ^{18}F -FDG PET/CT scans, enabling a comparison with the standard algorithm practiced at Institut Kanser Negara (IKN). The standard reconstruction method employed in the Nuclear Medicine Department of IKN involves the Q.Clear reconstruction algorithm with a beta value of 450, incorporating “Motion Free” (MF) (PET digital gating) and “Q.Static” (QS) for respiratory motion management. Additionally, the image reconstructed with beta values of 600 and 1000 are acquired simultaneously as backup options at IKN.

1.2. Problem Statement

The task relevant to oncologic PET imaging involves detecting a focal warm lesion against a noisy background. While the BPL reconstruction algorithm has demonstrated improvements in SNR and lesion quantitation accuracy, especially SUV recovery compared to OSEM (Teoh *et al.*, 2015, 2016), concerns persist regarding the potential over-smoothing effect of edge-preserving techniques on lesions, particularly low-contrast lesion. In other words, increasing beta values in the BPL algorithm may cause small lesions to blur into the background, thereby reducing their detectability. This phenomenon was observed in a study by Rijnsdorp, Roef & Arends (2021), particularly in Gallium-68 Prostate-Specific Membrane Antigen (^{68}Ga -PSMA) imaging, where higher beta values led to increased noise suppression but decreased detectability of small lesions, making them difficult to distinguish from the surrounding background (Wangerin *et al.*, 2017).

This study aims to evaluate quantitative and qualitative accuracy resulting from various beta value in BPL reconstruction for TOF and non-TOF ^{18}F -FDG PET/CT image quality. The limitations posed by the finite spatial resolution in PET imaging, along with issues like Partial Volume Effect (PVE), lead to poor lesion detection, compromised quantitative accuracy, and overall diagnostic quality. PVE becomes even more problematic when image contrast deteriorates due to blurring, hampering the early detection of small lesions and impeding the precise localisation of focal radiotracer uptake in the body. The suitability of beta value in BPL algorithm should be extensively explored, as it significantly affects metrics such as SNR and CNR. Higher beta values reduce noise but also lower contrast and SUV accuracy, while excessive noise can compromise the precision of SUV measurements (Wu, Guo, Huang, Zhao, *et al.*, 2021). Therefore, achieving the delicate balance between noise reduction, spatial resolution and contrast

enhancement remains a complex task, underscoring the importance of studying the optimal application of the BPL algorithm, particularly the beta value.

1.3. Study Objective

1.3.1. General Objective

The aim of this study is to evaluate the quantitative and qualitative accuracy resulted by various beta values in BSREM method between TOF and non-TOF ^{18}F -FDG PET/CT image quality and define the optimal value of each.

1.3.2. Specific Objectives

1. To quantitatively determine the effects of beta values to the Recovery Coefficient (RC), noise and CNR in TOF and non-TOF ^{18}F -FDG PET/CT.
2. To qualitatively measure the effect of beta values to the observer detectability.
3. To define optimal beta value for TOF and non-TOF ^{18}F -FDG PET/CT and compare its significance difference with the standard beta value practised at IKN.

1.4. Study Hypothesis

1.4.1. Null Hypothesis

1. Beta value has no effect on RC, noise and CNR between TOF and non-TOF ^{18}F -FDG PET/CT.
2. Beta value has no effect on observer detectability in TOF and non-TOF ^{18}F -FDG PET/CT.
3. There is no significant difference between the optimal beta value and the standard beta value practiced at IKN.

1.4.2. Alternative Hypothesis

1. Beta value has an effect on RC, noise and CNR between TOF and non-TOF ^{18}F -FDG PET/CT.
2. Beta value has an effect on observer detectability in TOF and non-TOF ^{18}F -FDG PET/CT.
3. There is a significant difference between the optimal beta value and the standard beta value practiced at IKN.

1.5. Significance of the Study

This study makes a significant contribution in defining an optimal image reconstruction protocol for ^{18}F -FDG PET/CT imaging, particularly focusing on the beta regularisation parameter in the BPL algorithm. Through quantitative and qualitative evaluation, the optimal reconstruction algorithm can enhance the diagnostic accuracy of imaging modalities, enabling physicians to access more informative images and make precise diagnostic decisions. Moreover, this study can guide healthcare institutions in customising their PET/CT imaging protocols, leading to more reliable and clinically meaningful results. The findings of this study are believed to contribute significantly to the Nuclear Medicine Department of IKN, as it compares the significant difference in the optimal reconstruction protocol and the standard image reconstruction protocol used in IKN. However, the choice of reconstruction protocol ultimately rests with IKN's preferences. Furthermore, the research findings have the potential to significantly enrich the curricula of academic institutions, particularly those offering programs related to medical imaging and radiology. Integrating these findings into coursework would provide students with practical insights into optimising imaging protocols, equipping them with the knowledge and skills required for their future careers. Additionally, this study can

serve as inspiration for other researchers to investigate reconstruction protocols for different radiotracers, given the limited number of local studies published on this topic.

CHAPTER 2

LITERATURE REVIEW

2.1. PET Imaging

Despite advances in morphological imaging techniques for detecting and monitoring malignancies over the past decades, limitations remain in diagnostic accuracy. Functional imaging, such as PET, has enhanced the sensitivity and specificity in diagnostic accuracy. PET is an analytical imaging technology designed to visualise and measure biochemical processes within living organisms using compounds labelled with positron-emitting radioisotopes (Huang *et al.*, 2017). It stands out for its capability to precisely quantify regional blood flow, metabolic activity, and organ function (Lammertsma, 2017). Quantification in PET imaging is essential for various clinical purposes, including defining biodistribution, evaluating dosimetry, making intra- and inter-individual comparisons, and establishing age- and gender-specific normative databases.

2.1.1. PET Radiotracers

The development of PET radiotracers for oncological applications is as important as the technological advances in PET devices. Their clinical uses differ significantly from country to country, partly due to the differences in regulatory agencies involved in controlling these radiotracers. ^{18}F -FDG is a widely used positron-emitting radiotracer in PET imaging, valuable for diagnosing and monitoring a broad range of conditions by visualising metabolic and biochemical activities in tissues. As a glucose analogue, FDG concentrates in cells with high energy demands, making it particularly effective for detecting tumours and areas of inflammation, which typically exhibit glucose uptake.

Currently, a variety of radiotracers are readily available to evaluate the same disease. For instance, in diagnosing prostate cancer, options include Fluorine-18 Prostate-Specific Membrane Antigen (^{18}F -PSMA) and ^{68}Ga -PSMA (Kroenke *et al.*, 2021) while for neuroendocrine tumours, alternatives include Gallium-68 DOTA-DPhe1-Tyr³-Octreotate (^{68}Ga -DOTA-TATE), Lutetium-177 DOTA-DPhe1-Tyr³-Octreotate (^{177}Lu -DOTA-TATE) and Fluorine-18 Silicon Fluoride Acceptor tagged Tyr³-octreotate (^{18}F -SiFAlin-TATE) (Ilhan *et al.*, 2020).

Besides, ^{18}F -L-dihydroxyphenylalanine (^{18}F -DOPA), originally developed to evaluate the dopamine transporter system in the striatum, has evolved into a versatile tool for assessing various diseases. It is particularly valuable in Parkinson's disease diagnosis (Blokhin *et al.*, 2024) and brain tumour imaging. Recently, it has been increasingly utilised in tumours of neural crest origin, aiding in detection, staging, and monitoring. In medullary thyroid cancer, its application shows promising results in staging.

Moreover, Carbon-11 Methionine (^{11}C -MET) PET imaging demonstrated high efficacy in detecting recurrent low-grade gliomas, outperforming FDG PET scans. A target-to-non-target ratio cut-off value of 1.47 serves as a valuable diagnostic parameter for distinguishing between benign and malignant lesions on ^{11}C -MET scan (Sharma *et al.*, 2016). Furthermore, ^{11}C -MET PET exhibits superior sensitivity and accuracy compared to magnetic resonance imaging (MRI) in predicting tumour recurrence in patients with previously treated paediatric high-grade gliomas. Notably, this imaging modality held potential prognosticating overall survival in this patient population (Bag *et al.*, 2022).

2.1.2. PET/CT Integration

Prior to the advent of hybrid technology, clinicians often faced challenges in accurately matching PET images with Computed Tomography (CT) images to locate and characterise lesions. This issue was addressed with the creation of the first PET/CT prototype by electrical engineer Ronald Nutt and physicist David Townsend in Switzerland, which was completed and installed at the University of Pittsburgh Medical Centre in 1998 (Maffione *et al.*, 2014). Time Magazine recognised PET/CT as the "Medical Science Invention of the Year" in 2000, highlighting its significance as a powerful new diagnostic tool (Jaroff, 2000). The integration of PET and CT technologies combines the functional insights of a PET scan with the detailed anatomical information from a CT scan in a single comprehensive examination. Consequently, this hybrid system enhances disease diagnosis and localisation which leads to earlier and more accurate diagnoses. For instance, PET/CT is particularly valuable in staging non-small cell lung cancer (Martucci *et al.*, 2020), assessing lung cancer recurrence and metastasis (Kandathil *et al.*, 2019), and developing radiation treatment strategies. The primary advantages of this integration are attenuation correction and precise anatomical localisation, significantly improving clinical outcomes. CT-based attenuation correction reduces whole-body imaging time by over 40% and creates a noiseless attenuation correction factor compared to standard PET transmission attenuation correction factors. To apply CT-based attenuation correction for PET images, the pixel intensities given in Hounsfield unit (HU) from CT scans are converted into linear attenuation coefficients (μ) suitable for PET's 511 keV energy level, typically achieved through bilinear fitting of attenuation coefficients against CT values across a range of x-ray energies. However, PET/CT does have limitations, including limited soft tissue contrast and additional radiation exposure from the CT component.

2.1.2.1 ¹⁸F-FDG PET/CT

The clinical use of PET/CT with FDG extends beyond oncological applications to encompass a variety of clinical conditions. FDG is a radiotracer that selectively accumulates in metabolically active cells, including those involved in infection and inflammation. This is due to increased glycolytic activity in inflammatory cells like neutrophils, lymphocytes, and macrophages, facilitated by increased levels of glucose transporter proteins and glycolytic enzymes (Zhuang & Codreanu, 2015). Therefore, FDG PET/CT becomes an indispensable tool for imaging granulomatous diseases, fungal infections, and other inflammatory conditions (Zhao *et al.*, 2019; Zhuang & Codreanu, 2015). While FDG PET/CT is highly useful in detecting abnormal metabolic activity, it has notable limitations because of the non-specific nature of elevated FDG uptake. Most human cells metabolise glucose for Adenosine Triphosphate (ATP) synthesis, leading to widespread physiological FDG uptake throughout the body. This can make it challenging to distinguish between infection, inflammation, and malignancy, all of which cause elevated FDG uptake. For instance, the uptake can be high in post-surgical granulation tissues or in response to sterile inflammation around implanted materials, such as vascular grafts, potentially leading to misinterpretation as an infection.

In addition, ¹⁸F-FDG PET/CT is emerging as a valuable imaging modality for evaluating cardiovascular inflammatory diseases. The accumulation and distribution of ¹⁸F-FDG at sites of inflammation or infection correlate with the severity and extent of the inflammatory or infectious process. FDG PET/CT is particularly crucial for monitoring disease activity and treatment response, especially in cardiac sarcoidosis. Skali *et al.* (2013) highlighted the significant role of ¹⁸F-FDG in both diagnosing and classifying patients with cardiac sarcoidosis. Moreover, ¹⁸F-FDG PET/CT is considered a reliable diagnostic tool for the detection of recurrence in colorectal cancer patients. It is

particularly favourable for patients with an unexplained increase in serum carcinoembryonic antigen level following primary curative treatment, as it changes the course of management in 59% to 68% of the patients (Almuhaideb *et al.*, 2011). Besides, FDG PET/CT significantly influence treatment decisions, often leading to a revision of the initial staging and affecting therapeutic strategies (Hadebe *et al.*, 2023). As reported by Almuhaideb, Papathanasiou & Bomanji (2011), ¹⁸F-FDG PET/CT changes the initial clinical staging and Tumour, Nodes, and Metastases (TNM) classification of tumours in a notable proportion of patients, ranging from 14% to 57%, compared with reliance on CT imaging for diagnosis alone.

However, FDG PET/CT has significant limitations related to its preparation and procedural time requirements. Patients are required to fast for 4 to 6 hours prior to the scan to minimise background FDG uptake and enhance the lesion-to-background ratio. The 110-minute half-life of ¹⁸F-FDG necessitates prompt synthesis and administration of tracers. Following intravenous injection, patients must remain still for approximately one hour to allow for proper biodistribution of FDG, thereby reducing the likelihood of non-specific uptake in skeletal muscles due to movement (Pijl *et al.*, 2021). Additionally, the effectiveness of FDG PET/CT can be significantly influenced by various medical drugs and conditions. Blood glucose levels must be below 11 millimoles per litre (mmol/L) for optimal results, which is challenging for diabetic patients, especially those on insulin. Insulin administration should be carefully timed to avoid interference, and metformin may induce increased intestinal FDG uptake (Hamidizadeh *et al.*, 2018), obscuring pathological findings. Besides, kidney failure may affect FDG excretion and background activity (Toriihara *et al.*, 2015), while liver failure can lead to increased hepatic FDG uptake.

2.2. Qualitative accuracy of PET/CT

Qualitative accuracy denotes the fidelity with which an imaging system delineates anatomical structures and pathological findings without distortion or artifacts. This precision is of immense importance for clinical interpretation, providing objective insights into disease progression, treatment response, and prognostic indicators. Albeit qualitative evaluation suffices for staging and post-treatment evaluation, quantitative analysis becomes indispensable for predicting tumour response during treatment. For example, qualitative interpretation of ^{18}F -FDG images helps differentiate between benign neurofibromas and malignant peripheral nerve sheath tumours in patients with neurofibromatosis type 1 (Chirindel *et al.*, 2015). It ensures that images accurately reflect the true biological and physiological processes within the body, without reliance on lesion SUV measurement or fixed thresholding (Chirindel *et al.*, 2015).

2.2.1. PET/CT Image Quality

The evaluation of PET images presents numerous challenges in routine clinical practice, primarily involving visual criteria to assess generalised or focal pathologies based on tracer accumulation. Inter-rater variability significantly limits the reliability of PET imaging, as studies demonstrate varying levels of agreement among readers using standardised criteria such as the Deauville score for lymphoma assessment (J. M. M. Rogasch *et al.*, 2022). However, reader training and discussions about differing interpretations have been shown to increase agreement, even among experienced readers (Ceriani *et al.*, 2017).

Subjective image quality is contingent upon both lesion contrast and image noise. Different readers may have varying preferences, with some favouring smoother images with less noise, even if this means potentially reduced lesion contrast. This variability

highlights the challenges inherent in qualitative image evaluation (J. M. M. Rogasch *et al.*, 2022). Interestingly, quantitative accuracy does not necessarily mandate optimal subjective image quality, as evidenced by consistent lesion SUV and detection rates in ^{18}F -FDG PET scans despite declining subjective image quality. Therefore, achieving high qualitative accuracy necessitates careful consideration of factors such as image resolution, noise reduction, and artifact minimisation during acquisition and reconstruction. Standardised quality control and quality assurance procedures are imperative to ensure consistent image acquisition standards across institutions, facilitating quantitative assessments for tumour response and radiotherapy planning.

2.3. Quantification accuracy of PET/CT

Quantification accuracy in PET/CT imaging is pivotal for both clinical diagnosis and research endeavours. This accuracy relies on various factors, including precise scanner calibration, data corrections, and advanced image reconstruction techniques. The quantification process provides significantly richer information compared to mere visual interpretation of images, particularly in differential diagnosis, where parameter values with certain thresholds aid in accurate diagnosis. It is also crucial in prognosis, as the physiological parameter values play a decisive role in staging patients. In therapeutic management, accurate quantification is indispensable, notably for post-therapy follow-up and radiotherapy planning. Continuous technological advancements and methodological improvements further enhance PET/CT's ability to provide accurate quantification, solidifying its indispensable role in modern oncology and other clinical practices.

2.3.1. Quantitative metrics of PET/CT

The evaluation of image quality in PET/CT scans is intricate and influenced by both biological and physical factors (Fukukita *et al.*, 2014). It can be assessed using various quantitative metrics such as SNR, CNR, SUV, and uniformity of specific target regions like lesions or healthy liver sections. These parameters provide reproducible values that rely on regular quality tests to analyse performance of imaging unit.

Understanding the interplay among spatial resolution, contrast, and noise is imperative for improving image quality in PET/CT imaging and ensuring accurate diagnostic accuracy and optimal treatment planning for oncology patients. Spatial resolution refers to the ability of an imaging system to resolve fine details of the object being studied. PET scanners typically exhibit lower spatial resolution compared to other morphological imaging modalities like CT and MRI. The spatial resolution of a PET system is typically characterised by a Point Spread Function (PSF), which is described in terms of its full width at half maximum along three orthogonal axes (radial, tangential, and axial) with reference to the cylindrical geometry of the PET detector arrangement (F. L. Andersen *et al.*, 2013). Spatial resolution is influenced by various factors, such as detector size (width), positron range (Jodal *et al.*, 2012), non-collinearity of emitted annihilation photons, and other system-specific characteristics, as reported by Moses (2011).

Despite ongoing advancements in PET design, spatial resolution remains limited to approximately 4 – 6 mm (Zaidi & Becker, 2016). FDG PET imaging lacks the necessary resolution for intricate structural details regarding tumour extension and involvement of adjacent structures. This limitation can result in the oversight of superficial lesions and low-grade tumours, particularly in areas with significant physiological FDG uptake nearby. Consequently, the limited resolution may lead to the

non-detection of small malignant tumours and metastases lymph nodes, causing false-negative results due to PVE and a decrease in perceived SUV (Purohit *et al.*, 2014).

On the other hand, contrast in PET images reflects the differences in pixel intensities between various radioactive concentration levels, which is crucial for distinguishing lesions from the surrounding background. Lesions appear as "hot" or "cold" areas in the image, indicating high or low levels of radioactivity uptake in those regions, respectively. Clinical PET images often exhibit higher levels of noise compared to other imaging modalities. Image noise not only detracts from the observer interest but also hinders the visualisation of essential diagnostic features. However, in some cases, image noise can be important for tumour detection. One of the factors that considerably affects both the intensity and texture of noise present in the images is reconstruction algorithm, which was discussed in detail in the Section 2.4.2. Additionally, increasing activity concentration results in improved image uniformity, where variations or inconsistencies across the image are reduced, which is associated with a lower noise level (Hasford *et al.*, 2016).

In PET/CT imaging, CNR and SNR are the main parameters for image quality. CNR measures the relative strength of the contrast between different regions or structures in an image compared to the background noise level. Higher CNR values can enhance detection sensitivity and facilitate earlier diagnosis by preserving spatial resolution while retaining noise within acceptable levels in a clinical setting. Conversely, SNR focuses on the ratio of the signal intensity to the standard deviation of the noise, reflecting the overall clarity and reliability of the signal present in the image. In simple terms, a high-SNR image exhibits a clearer differentiation between the actual signal of interest, such as tumour activity, and the surrounding noise in the image. However, achieving a high SNR in PET imaging can be challenging due to inherent factors such as scattered coincidences,

random coincidences, and the application of random corrections, as well as limitations in spatial resolution and image sampling. To achieve satisfactory SNR in PET images, filtering methods can be employed either during the image reconstruction process, where a prior term is incorporated into the statistical reconstruction algorithm, or post-reconstruction through filtering techniques. Despite a particular image having a high SNR, its diagnostic utility remains limited unless accompanied by a sufficiently high CNR to distinguish between different tissue types, including healthy and pathological tissue.

SUV is a semiquantitative measure without a specific unit, used to quantify tracer uptake and infer the potential malignancy of a region. It refers to the ratio of activity per unit volume within a region of interest (ROI) to the activity per unit volume across the entire body. This calculation relies on a precise knowledge of the injected dose quantity, timing and patient size. Various SUV formulas exist, differing in their normalization methods (e.g., by weight, lean body mass, or body surface area) and ROI analysis approaches (e.g., SUV_{max} , SUV_{mean} , SUV_{peak}). However, it is widely recognised that SUV alone in FDG PET is insufficiently for definitively distinguishing between malignant and benign lesions. Other factors play crucial roles in this evaluation, including the lesion's location and size, CT morphology, contrast enhancement pattern, and symmetry. Additionally, SUV values depend on many patient-related factors such as plasma glucose levels, competition with endogenous glucose, phosphorylation rate, body size and body composition, as well as the tumour type.

FDG uptake and SUV values does not always reliably indicate malignancy. Some benign infectious or inflammatory processes can show intense FDG uptake and high SUV values. Conversely, certain indolent or slow-growing malignant processes might display minimal FDG uptake and low SUV values. From a technical standpoint, several factors

can affect SUV measurements. These include the PET scanner's ability to distinguish signal from noise, the accuracy of image reconstruction and correction algorithms, and the timing between tracer injection and image acquisition. Failing to account for these various sources of error can result in significant inaccuracies in SUV calculations, potentially leading to discrepancies of 50% or more.

2.4. Factors affecting PET Image

Factors affecting PET image quality include a multitude of intrinsic and extrinsic variables that influence the accuracy and reliability of PET imaging. These factors, including radiotracer properties, dose administration, reconstruction algorithms, and the PVE, are crucial in shaping the clarity, precision, and diagnostic value of PET scans. Therefore, a thorough understanding of these factors is essential to ensure that findings from PET imaging remain consistent and accurate across different studies and clinical settings.

2.4.1. Radiotracer properties and dose administration

Radiotracers exhibit varying biokinetics and affinities, influencing their distribution within the body and their ability to bind to specific targets (Kotzerke & van den Hoff, 2017). These differences in radiotracer properties can affect the detectability of small lesions and overall image quality. In addition, the process of PET image reconstruction is complicated by the dependence of radiotracer distribution on the patient's physiology and constitution (J. M. M. Rogasch *et al.*, 2022). Moreover, the spatial resolution and image quality of a digital PET/CT scan are influenced by the positron energy emitted by the PET nuclide. Braune *et al.* (2022) reported that PET/CT images obtained with ^{18}F -FDG or Copper-64 Hydrochloric acid (^{64}Cu -HCl) tend to have

superior image quality and spatial resolution compared to those obtained with Gallium-68 Hydrochloric acid ($^{68}\text{Ga-HCl}$), despite similar count rates.

The effective administration of a radiotracer dose is crucial for obtaining high-quality PET images and reliable quantification of PET data (Plaxton *et al.*, 2014). The European Association of Nuclear Medicine (EANM) procedure guidelines have outlined standardised protocols for administering radiotracers, such as $^{18}\text{F-FDG}$, and acquiring whole-body PET scans to ensure consistency across different imaging systems and centres. However, efforts to standardise doses administration based on patient characteristics, such as body weight, have encountered challenges, particularly in the case of obese patients. This issue can potentially lead to decreases image quality and false-negative PET scans. Research suggests that optimising the administered FDG dose based on patient-dependent parameters, such as Body Mass Index (BMI) or lean mass, may be necessary to achieve more uniform image quality (de Groot *et al.*, 2013). Furthermore, advancements in PET technology, such as TOF and position-dependent PSF reconstructions, may alter the optimal relationship between patient-dependent parameters and radiotracer dose, necessitating ongoing investigation to optimise PET imaging protocols and enhance image quality and quantification accuracy.

2.4.2. Reconstruction algorithm and parameters

The variation among PET/CT scanners and the different image reconstruction methods employed affects the quality and interpretation of PET images, consequently impacting the accuracy and reproducibility of SUV measurements. Recent advancements in PET technology have led to significant improvements in both hardware and software components. Modern PET systems feature enhanced detector materials and designs, as well as more sophisticated image reconstruction algorithms and correction techniques.

These upgrades have resulted in superior image quality and more accurate quantitative measurements. The process of PET image reconstruction involves complex mathematical operations. It transforms the raw data from multiple projections that originate from the coincident events detected by the scanner into three-dimensional (3D) tomographic images. These images reflect the spatial distribution of the radiotracer activity within the object, measured in terms of activity concentration (Bq mL^{-1}). While analytic image reconstruction methods work under the assumption that PET data is noise-free and provide a straightforward mathematical approach to image formation, iterative methods account for the statistical noise in PET data, leading to a more complex mathematical solution that requires multiple steps and significant computational power to produce the optimal image (Vrachliotis *et al.*, 2022).

2.4.2.1. Ordered Subset Expectation Maximisation (OSEM)

A commonly used algorithm in clinical settings is OSEM due to its reliability, commendable reconstruction, and optimal convergence rate. Instead of using the entire image dataset for each iterative image update, the process of forming an image can be accelerated by dividing the objective function into sub-objective functions using only a subset of data (Lindström, 2022). Compared to analytical reconstruction methods like filtered back projection, OSEM enhances the SNR while preserving the quantitative integrity of tomographic data (Chen *et al.*, 2024). It allows for accelerated reconstruction by modelling various system factors such as PSF and TOF. As a result, OSEM is widely regarded as the gold standard for statistical image reconstruction algorithm (Chicheportiche *et al.*, 2021).

However, the main drawback of OSEM is a trade-off between the number of subsets, iterations, and image quality. When the number of subsets is increased, noise and

artifacts can also increase because each subset contains limited tomographic and statistical information (van der Vos *et al.*, 2017). Additionally, more iterations result in higher background noise, reducing accuracy and image quality. Thus, the OSEM reconstruction process is stopped early to prevent excessive noise buildup. In clinical practice, post-filtering techniques are applied to ensure satisfactory image resolution and adequate SNR.

2.4.2.2. Bayesian Penalised Likelihood (BPL)

Q.Clear, also known as BPL, is an advanced reconstruction algorithm introduced by General Electric (GE) Healthcare. It includes PSF modelling and different innovative penalty functions to enhance image quality and suppress noise in PET imaging, as demonstrated in Figure 2.1. Unlike traditional methods like OSEM, Q.Clear integrates an additional term into its objective function that increases with image noise, thereby steering the optimisation process away from noisier images (Ross, n.d.). This algorithm utilises the RDP to apply activity-dependent smoothing and noise suppression in low-activity background regions, with a fixed penalty factor of 2 (Ahn *et al.*, 2015). It achieves superior image quality without compromising on edges preservation (Matti *et al.*, 2019). The BSREM algorithm allows each voxel to achieve 100% convergence for consistent and reliable results across the image. By modulating regularisation, Q.Clear strikes an optimal balance between image quality and quantitation, preserving edges while minimising background noise.

Moreover, Q.Clear operates without the need for post-filters, as noise control is integrated into the iterative reconstruction process. This approach results in improved SNR and SUV measurements, which is particularly beneficial for detecting small lesions in clinical scans. Nonetheless, appropriate parameters such as the noise penalty factor

must be carefully considered to achieve the desired balance between noise suppression and edge detection. High beta values result in stronger noise suppression, but on the other hand, it can affect other things like edge detection and volume determination (Parvizi *et al.*, 2015).

BSREM has been shown to provide better quantitation accuracy than OSEM in phantom studies and clinical studies with simulated lesions (Ahn *et al.*, 2015). Several studies revealed that the advantages of the BPL algorithm for evaluating small pulmonary nodules (Howard *et al.*, 2017; Teoh *et al.*, 2016), liver metastases (Teoh *et al.*, 2015), and mediastinal nodes in non-small lung cancer cells. Beta values of 300 and 500 were recommended for smaller and larger lesions, respectively (Sadeghi *et al.*, 2023), with 400 being the preferred choice for clinical use (Howard *et al.*, 2017; Teoh *et al.*, 2015). This selection was shown to depend on factors such as lesion size and tumour-to-background ratio (TBR) (Sadeghi *et al.*, 2023).

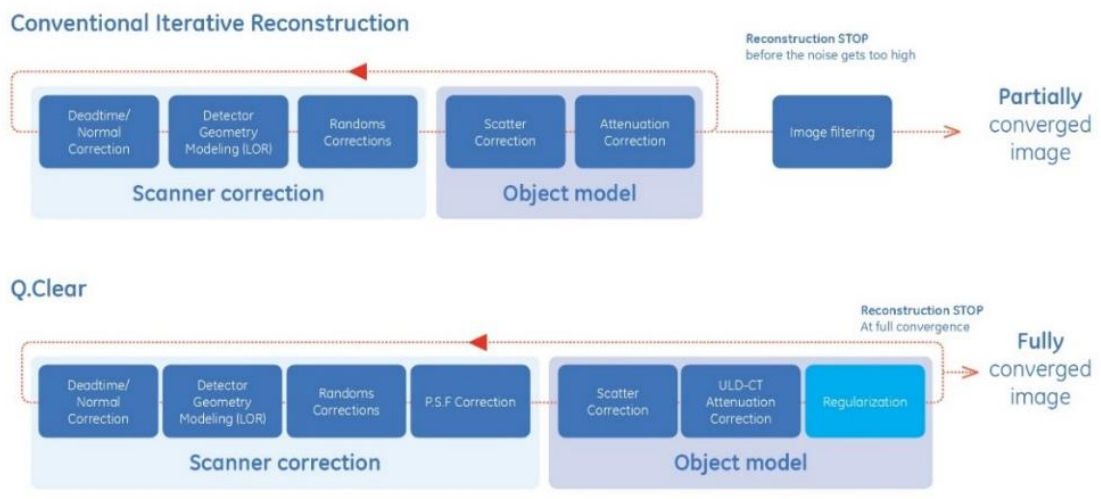


Figure 2.1: Process flow maps for conventional OSEM iterative reconstruction and Q.Clear (Ross, n.d.).

2.4.2.3. Point Spread Function (PSF)

Iterative reconstruction allows system properties to be included into the reconstruction process. The PSF reconstruction technique has become commercially available for PET imaging. It corrects for photon mispositioning, known as the parallax effect, occurring as gamma rays pass through the scintillation detectors at various angles (non-oblique and oblique angles) as well as for inter-crystal scattering, positron range, and photon non-collinearity (Hotta *et al.*, 2018). Resolution recovery modelling, which is derived from point source measurements at different positions within the scanner's field of view, describes the relationship between image space and projection space (Lindström, 2022). The resulting PSF is then represented in the system matrix and may include factors such as depth-dependent sensitivity and spatially variant detector response (Alessio *et al.*, 2010). This PSF can be obtained from simulations, analytical calculations, or point source measurements. This approach enhances the spatial resolution and SNR of PET images, thereby increasing the detection sensitivity for small lesions. However, PSF-based reconstruction may introduce edge artifacts, known as Gibb's artifacts, which can affect quantitative accuracy (Nuyts, 2014).

2.4.2.4. Time-of-Flight (TOF)

Although the concept of using TOF information dates back to the introduction of PET in the 1960s, the first commercial PET system incorporating TOF technology was launched in 2006 (Lindström, 2022). In PET imaging, the signal is generated through the annihilation of a positron with an electron in the surrounding medium or tissue. TOF technology precisely measures the difference in the arrival times of the two 511 keV photons produced by positron annihilation, as illustrated in Figure 2.2. This TOF

information is then used to localise the annihilation point along the line of response, with the distance from the line of response centre point determined by Equation (1):

$$d = c \frac{\Delta t}{2} \tag{1}$$

where c is the speed of light in vacuum and Δt is the time difference between detection of photons. Therefore, TOF information is considered to reduce the noise and to improve the contrast (Lois *et al.*, 2010; Vandenberghe *et al.*, 2009).

Even though knowledge of emission point locations along the line of response is not necessarily required for reconstruction, leveraging TOF can significantly improve accuracy by imposing precise timing constraints on potential emission event locations. Studies by Turkington & Wilson (2009) and Conti (2011b) have proved that TOF PET images are more robust, being less sensitive to error in data correction techniques such as normalisation, scatter and attenuation correction. Furthermore, TOF data acquisition enables iterative image reconstruction to converge more rapidly and withstand inconsistencies, incompleteness, or inaccuracies in the data.

TOF sensitivity gain is inversely proportional to the detector timing resolution (Surti, 2015). In simpler terms, a shorter coincidence timing resolution of the system further enhances localisation accuracy, resulting in greater improvement in SNR (Lindström, 2022). The study reported by Surti & Karp (2009) indicated that as the timing resolution improves in TOF PET, there is enhanced detectability of lesions in uniform objects. The primary motivation for TOF PET has always been to improve image quality or reduce image acquisition time, with the greatest benefits observed in heavier patients who typically experience poorer image quality. TOF reduces patient-size dependence and allows for a reduction in the administered radiotracer dose or scan time (Surti, 2015). Recent studies have demonstrated that TOF significantly improves image quality,

especially for heavier patients with lower contrast lesions (El Fakhri *et al.*, 2011; Surti *et al.*, 2011). A clinical study has proved that TOF information helps improve the image quality of overweight patients to a level closer to that of normal-weight patients (Conti, 2011a). Besides, Lois *et al.* (2010) reported that the SNR gain from TOF had the greatest effect in patients with higher BMI. Their study demonstrated that incorporating TOF information resulted in improvements in image detail resolution, enhanced definition of small lesions, and image uniformity.

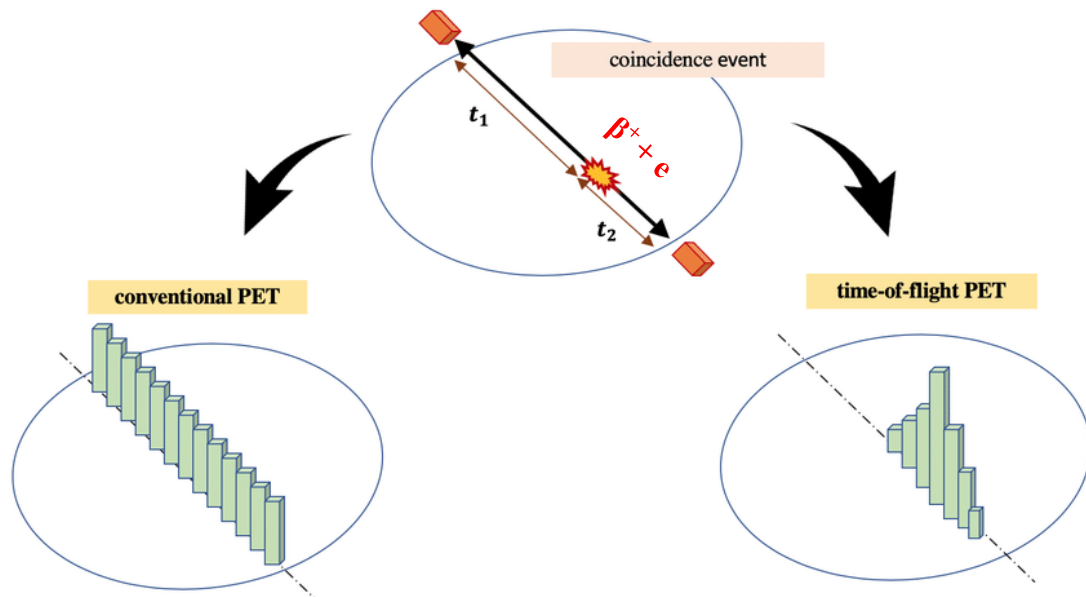


Figure 2.2: Schematic illustration of conventional PET and TOF PET (Brusaferrri, 2020).

2.4.3. Partial Volume Effect (PVE)

Despite advancements in scanner technology and reconstruction algorithms, the PVE continues to be a major challenge, significantly impacting the resolution and quality of PET images. PVE is a well-documented phenomenon present in nearly all medical imaging data, where measured radioactivity concentrations appear lower than their true values. This discrepancy poses a significant challenge in establishing accurate dose-response relationships for radionuclide therapies, particularly when targeting specific